Domains 12 to 16 of tropoelastin promote cell attachment and spreading through interactions with glycosaminoglycan and integrins alphaV and alpha5beta1

Brigida Bochicchio[1], Giselle C. Yeo[2,3], Pearl Lee[2,3], Deniz Emul[2,3], Antonietta Pepe[1], Antonio Laezza[1], Nicola Ciarfaglia[1], Daniela Quaglino[4] and Anthony S. Weiss[2,3,5]

1 Department of Science, University of Basilicata, Potenza, Italy
2 Charles Perkins Centre, The University of Sydney, NSW, Australia
3 School of Life and Environmental Sciences, The University of Sydney, NSW, Australia
4 Department of Life Sciences, University of Modena and Reggio Emilia, Modena, Italy
5 Sydney Nano Institute, The University of Sydney, NSW, Australia

Elastin is an extracellular matrix component with key structural and biological roles in elastic tissues. Interactions between resident cells and tropoelastin, the monomer of elastin, underpin elastin's regulation of cellular processes. However, the nature of tropoelastin–cell interactions and the contributions of individual tropoelastin domains to these interactions are only partly elucidated. In this study, we identified and characterized novel cell-adhesive sites in the tropoelastin N-terminal region between domains 12 and 16. We found that this region interacts with αV and α5β1 integrin receptors, which mediate cell attachment and spreading. A peptide sequence from within this region, spanning domains 14 to mid-domain 16, binds heparan sulfate through electrostatic interactions with peptide lysine residues and induces conformational ordering of the peptide. We propose that domains 14–16 direct initial cell attachment through cell-surface heparan sulfate glycosaminoglycans, followed by αV and α5β1 integrin-promoted attachment and spreading on domains 12–16 of tropoelastin. These findings advance our mechanistic understanding of elastin matrix biology, with the potential to enhance tissue regenerative outcomes of elastin-based materials.

Introduction

The elasticity of organs and tissues in vertebrates is due to the presence of elastin, and an insoluble protein whose soluble monomer, tropoelastin, is enzymatically cross-linked through ε-amino groups of lysine residues. Tropoelastin assembly with other extracellular matrix (ECM) components, such as matrix-associated glycoproteins and fibrillins, gives rise to elastic fibers, which possess mechanical strength, elasticity, and cell-interactive properties [1].

Tropoelastin is known to interact directly with cells through cell-surface receptors including elastin-binding protein (EBP) [2], glycosaminoglycans (GAGs), [3] and integrins [4–6]. GAGs are negatively charged polysaccharides linked to cell-surface or ECM proteoglycans such as the members of the syndecan family. Due to their highly negative charges, GAGs can interact with positively charged amino acids such as lysines. Consistent with this model, a number of identified cell-

binding regions in tropoelastin contain such residues, such as the RKRK motif in domain 36 [4]. Recently, a two-step mechanism involving GAGs and integrins was shown for the central domains 17–18 of tropoelastin [7]. Domain 17 is one of the few lysine-rich regions in tropoelastin that does not participate in cross-linking, leaving the lysine residues available for cell-receptor interactions. Initial cell adhesion is proposed to be mediated by GAG-lysine contacts, while subsequent cell spreading is facilitated by integrins.

Glycosaminoglycans can be either sulfated or non-sulfated. Sulfated GAGs include chondroitin sulfate (CS), heparin, and heparan sulfate (HS). *In vitro* studies have shown that HS enhances the coacervation properties of tropoelastin to induce its aggregation into an ordered fibrillar structure, confirming the importance of GAGs in elastic fiber assembly [8].

Previous reports have implicated the presence of additional cell-binding sites in tropoelastin apart from domains 17–18 and domain 36 [7]. In this study, we reveal cell-interfacing motifs in the N-terminal region upstream of these domains. We also determine the cell-receptor mechanisms mediating interactions with this segment of tropoelastin. In particular, a sequence between domain 14 and mid-domain 16 appears to be important for initial cell contact. We synthesize this sequence, corresponding to residues 246–281 of human tropoelastin, and extensively characterize its cell-interactive properties at the molecular and supramolecular level.

Results

Cell-interactive site/s exist upstream of domains 17–18 of tropoelastin

Truncated tropoelastin constructs were used to understand the contribution of N-terminal tropoelastin domains to cell interactions (Fig. 1). The tropoelastin construct spanning the N terminus to domain 18 (N18) has previously been shown to be cell-adhesive, with a cell-binding sequence isolated to within domains 17–18 [7]. Shorter constructs—N16 (N terminus to domain 16) and N12 (N terminus to domain 12)—were synthesized to determine the existence of cell-binding capability upstream of domains 17–18. N12 includes a key region in domain 12, where a homozygous missense mutation of proline into serine at position 211 (P211S) is associated with mild cutis laxa (30). N10 (N terminus to domain 10), which is known to be noncell adhesive [7], serves as a negative control.

Human dermal fibroblasts adhered to both N18 and N16 in a dose-dependent manner (Fig. 2A). Cell

binding to N16 (61 ± 1.1%) was significantly lower than to N18 (76.9 ± 10.3%). N12 showed minimal levels of cell attachment similar to the N10-negative control. N16 supported cell spreading at 1 h (77.4 ± 1.5%), although again to a significantly lesser extent than N18 (87.3 ± 2.7%) (Fig. 2B). N12 did not allow cell spreading (4.5 ± 1%), as expected from its low cell attachment ability. Representative images illustrated that cells on N18 and N16 were predominantly spread with phase-dark nuclei, compared to cells on N12, which were predominantly unspread with phase-bright nuclei (Fig. 2B). While N18 displayed a higher degree of cell interactivity than N16, attributable to the previously reported cell-binding site within domains 17–18, N16 still exhibited evident cell-adhesive and spreading properties, strongly suggesting the presence of upstream cell-interactive site/s within domains 13–16 of tropoelastin.

Domains 12–16 support cell attachment and spreading through αV or α5β1 integrins

To validate the cell-interactive properties of these upstream domains, a tropoelastin construct spanning domains 12–16 was synthesized. At maximal concentrations, the 12–16 construct supported cell attachment (57.0 ± 5.0%) to the same level as N16 (50.7 ± 1.7%; Fig. 2C). Maximal cell adhesion was achieved at a lower concentration of 12–16 than N16, suggesting a higher efficiency of cell binding to 12–16. The 12–16 construct enabled cell spreading (75.3 ± 2.1%) comparably to N16 (77.4 ± 1.5%; Fig. 2D).

To determine the cell-binding mechanism/s, cell adhesion to the 12–16 tropoelastin construct was performed in the presence of lactose, HS, or EDTA as inhibitors (Fig. 3A). Inclusion of either lactose or HS posed no effect, while EDTA significantly inhibited cell attachment by 95.4 ± 0.3%, suggesting the primary involvement of integrins in this process.

To identify the specific integrins mediating cell attachment to 12–16, a panel of anti-integrin-blocking antibodies were deployed. Inclusion of the pan-anti-αV integrin inhibitory antibody 17E6 and the anti-α5β1 integrin antibody JBS5 separately did not inhibit cell attachment to 12–16. However, the combination of both antibodies inhibited cell attachment by 69.3 ± 11.7% (Fig. 3B), indicating that either type of integrin can facilitate cell adhesion to 12–16.

Blocking pan-anti-αV integrins significantly inhibited cell spreading on 12–16 by 59.1 ± 9.3%, while blocking the α5β1 integrin alone had no effect. Blocking both αV and α5β1 integrins further inhibited cell
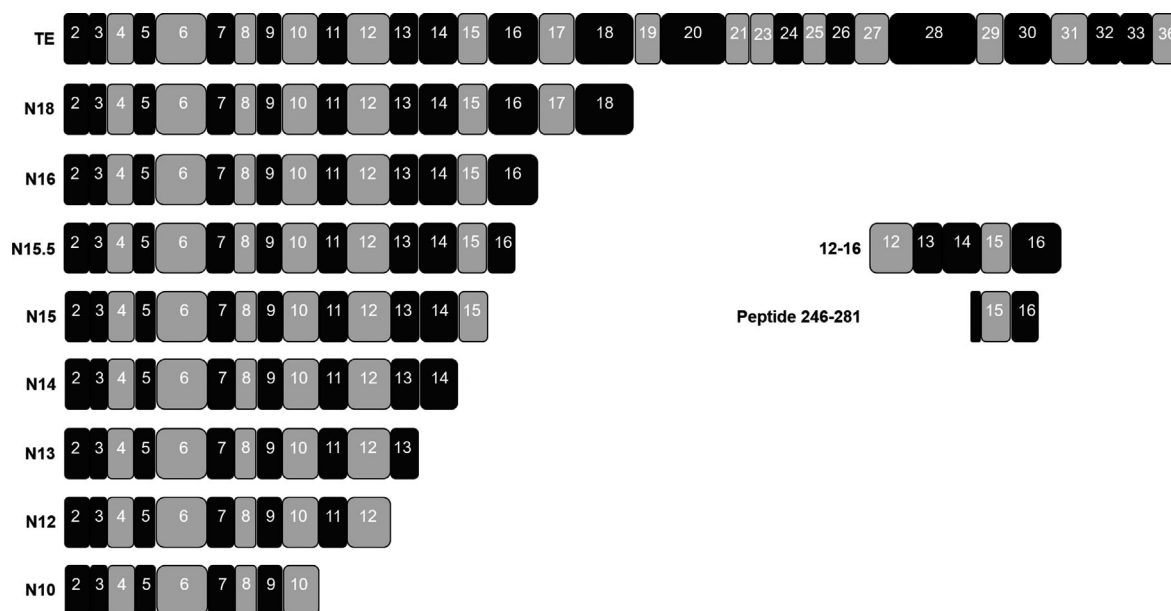
Fig. 1. Schematic representation of tropoelastin constructs used in this study. The light gray regions indicate hydrophilic domains, and the black regions indicate hydrophobic domains.
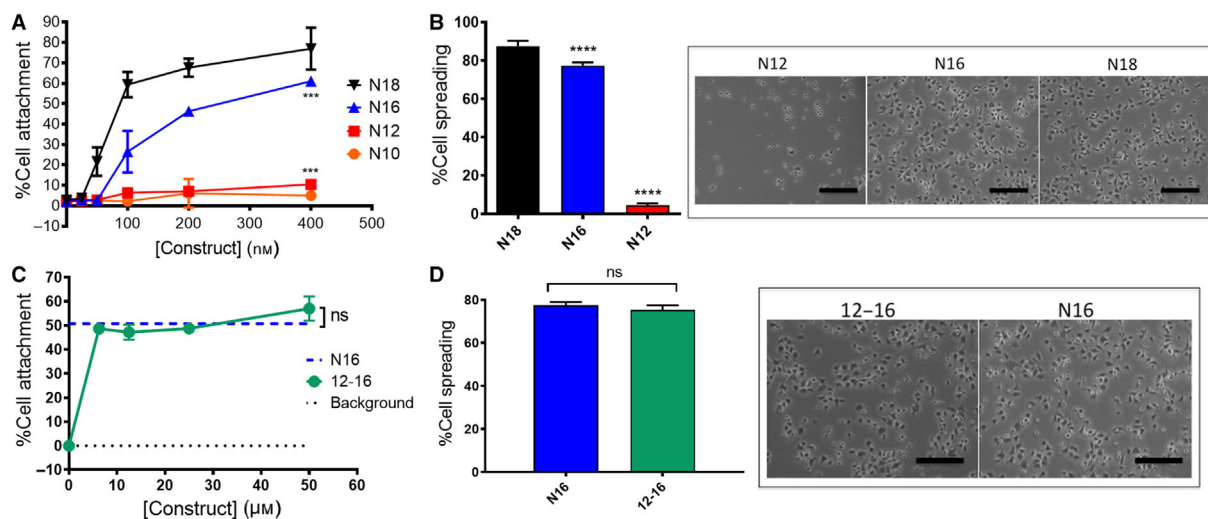
Fig. 2. (A) Cell adhesion to increasing molar concentrations of the tropoelastin constructs N18, N16, N12, and N10 ($n = 3$). (B) Cell spreading on N18, N16, and N12 ($n = 4$). (C) Cell adhesion to increasing molar concentrations of 12–16 with N16 as the positive control ($n = 3$). (D) Cell spreading on 12–16 and N16 ($n = 4$). Scale bar: 200 μm. Values are reported as mean ± SD. Statistical tests were carried out using ANOVA with Bonferroni post-test. ***$P < 0.001$; ****$P < 0.0001$.

spreading by 95.3 ± 5.6% (Fig. 3C). Inclusion of both antibodies at half the concentration did not diminish their inhibitory potential (Fig. 3D). These results lend further support to the roles of integrins αV and α5β1 in driving cell interactions. To confirm that the anti-α5β1 integrin JBS5 antibody was functional, it was used to successfully inhibit cell spreading on fibronectin, an integrin α5β1 ligand (Fig. 3E,F). The negative

control pan-anti-β8 integrin antibody did not inhibit cell spreading on both 12–16 and fibronectin.

Major cell-interactive site lies within domains 15 and 16

C-terminally truncated constructs N16, N14 (N terminus to domain 14), N13 (N terminus to domain 13),
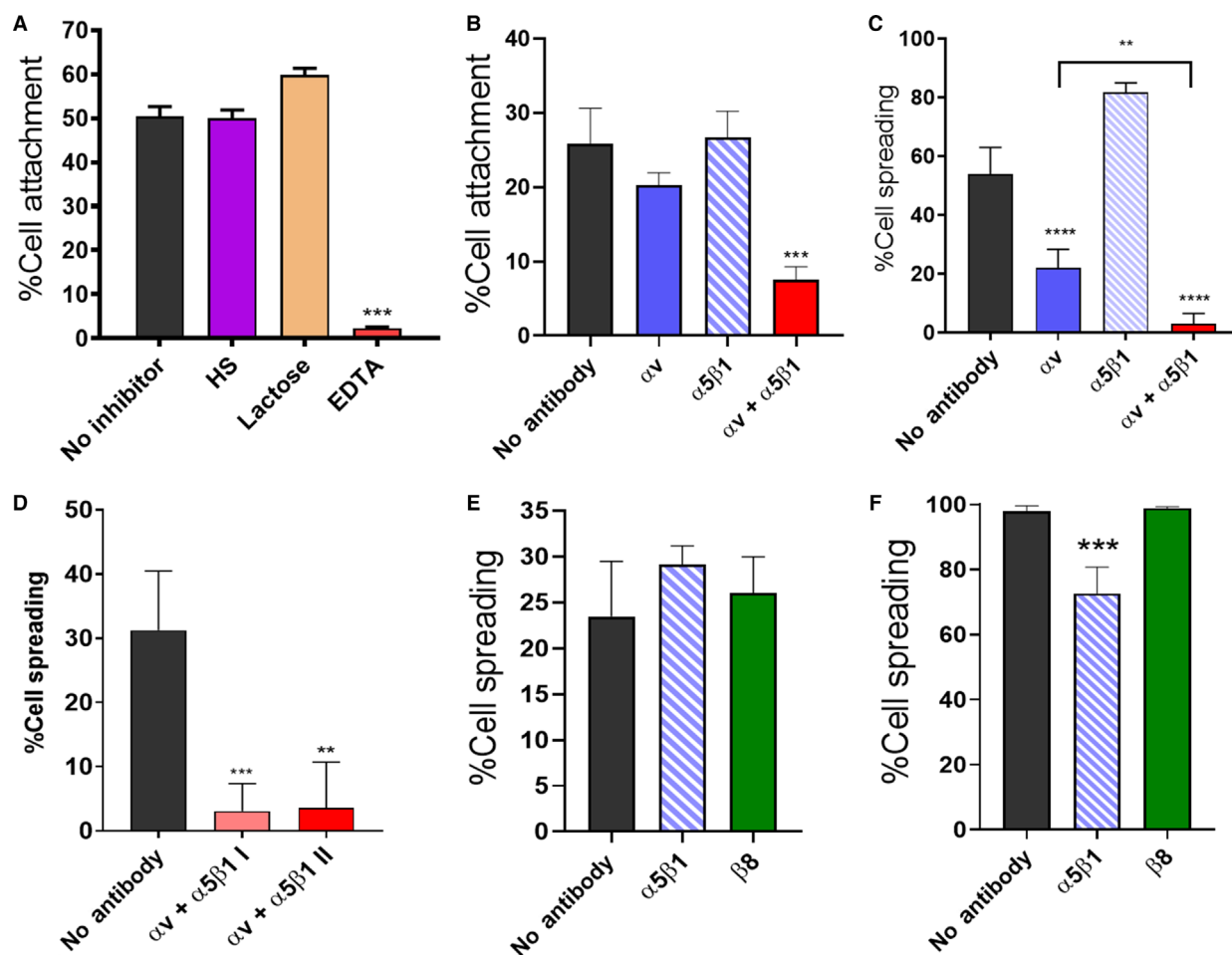
Fig. 3. Cell attachment to the 12–16 tropoelastin construct (A) in the presence of HS (10 µg·mL^{-1}), lactose (10 mM), or EDTA (5 mM); or (B) in the presence of the anti-αV integrin antibody (20 µg·mL^{-1}), anti-α5β1 integrin antibody (one in 50 dilution), or both antibodies ($n = 3$). Cell spreading on 12–16 in the presence of (C) anti-αV integrin, anti-α5β1 integrin, or both antibodies; (D) both antibodies at 20 µg·mL^{-1} and one in 50 dilution, respectively (αV + α5β1 I), or at 10 µg·mL^{-1} and one in 100 dilution, respectively (αV + α5β1 II) ($n = 4$). Cell spreading on (E) 12–16 and (F) fibronectin (FN) in the presence of anti-αV integrin (20 µg·mL^{-1}), anti-α5β1 integrin (1 in 50 dilution), or an antibody against integrin β8 (20 µg·mL^{-1}) ($n = 4$). Values are reported as mean ± SD. Statistical tests were carried out using ANOVA with Bonferroni post-test. **$P < 0.01$; ***$P < 0.001$; ****$P < 0.0001$.

and N12 were used to delineate the potential cell-binding regions within domains 13–16 (Fig. 4A). At maximal concentrations, N14 displayed significantly decreased cell binding (26.1 ± 4.5%) compared with N16 (52.1 ± 2%), indicating a dominant cell-adhesive site between domains 15–16 (Fig. 5). N14, N13, and N12 also slightly differed in their cell attachment abilities (26.1 ± 4.5%, 16.2 ± 2.9%, and 9.3 ± 0.1%, respectively), suggesting the possibility of additional cell-binding sites in domains 13–14. To explore these differences further, cell-spreading assays were carried out with these constructs over 1 h. Cell spreading on N14 (14.4 ± 5.7%), as on N13 (13.3 ± 3.7%), was significantly lower than that on N16 (65.3 ± 8.9%)

(Fig. 4B), reinforcing the presence of a major cell-interactive site within domains 15–16 of tropoelastin.

To further investigate this cell-binding site within domains 15–16, the construct N15.5, encompassing the N terminus to the first 15 residues of domain 16, was synthesized. Cell attachment to N15.5 (61.7 ± 9%) was significantly higher than that to N14 (27.4 ± 3.8%; Fig. 4C) and indistinguishable to N16 (Fig. 4D). Likewise, there was no significant difference between cell spreading on N15.5 (65.3 ± 2.7%) and N16 (59.8 ± 5.5%), both of which were higher than cell spreading on N14 (29.4 ± 7.4%; Fig. 4E). Collectively, these findings suggest that the cell-interactive region in N16 primarily lies within domain 15 and the first half of domain 16.
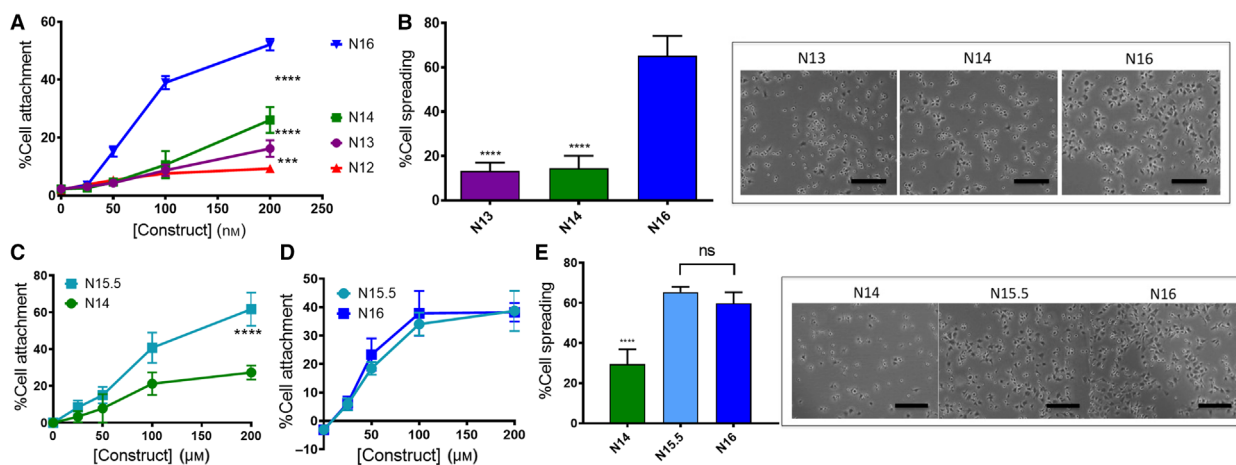
Fig. 4. (A) Cell adhesion to increasing molar concentrations of the tropoelastin constructs N16, N14, N13, and N12 ($n = 3$). (B) Cell spreading on N16, N14, and N13 ($n = 4$). (C) Cell adhesion to N15.5 and N14, and to (D) N15.5 and N16 ($n = 3$). (E) Cell spreading on N16, N15.5, and N14 ($n = 4$). Scale bar: 200 μm. Values are reported as mean ± SD. Statistical tests were carried out using ANOVA with Bonferroni post-test. ***$P < 0.001$; ****$P < 0.0001$.
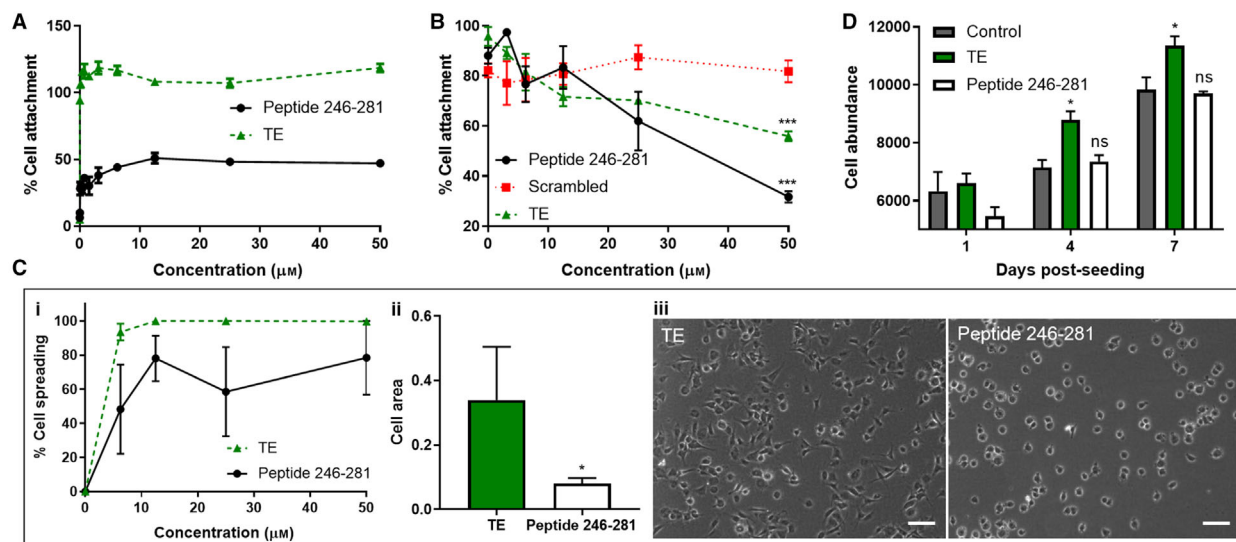

Fig. 5. (A) Adhesion of human dermal fibroblasts to tissue culture wells coated with increasing concentrations of peptide 246–281 or full-length tropoelastin (TE) ($n = 3$). (B) Inhibition of cell adhesion to a tropoelastin substrate by the addition of increasing concentrations of peptide 246–281, scrambled peptide, or tropoelastin in solution ($n = 3$). (C) Cell spreading on wells coated with increasing concentrations of peptide 246–281 or tropoelastin. The (i) extent of spreading, (ii) area of spread cells, and (iii) representative images of spread cells are shown ($n = 3$). Scale bar: 50 μm. (D) Cell proliferation over 7 days on uncoated tissue culture plastic (TCP), or TCP coated with 50 μM tropoelastin or peptide 246–281 ($n = 3$). Values are reported as mean ± SD. Statistical tests were carried out using ANOVA with Bonferroni post-test. *$P < 0.05$; ***$P < 0.001$.

Tropoelastin-derived peptide 246–281 supports cell attachment and spreading

On this basis, a peptide (peptide 246–281) was synthesized to span the last three residues of domain 14, the entire domain 15, and the first 15 residues of domain 16 in tropoelastin: TGTGVGPQAAAAAAA-KAAAKFGAGAAGVLPGVGGAG. Cell attachment

to peptide 246–281 alone was 40% of that to full-length tropoelastin (Fig. 5A), confirming that this peptide contains a major cell-binding site within tropoelastin. Furthermore, cell recognition of the peptide is sequence-specific and mirrors at least one type of cell interaction with the full-length protein. Peptide 246–281 significantly inhibited cell attachment to

tropoelastin by 64% at highest tested concentrations (Fig. 5B). In fact, peptide 246–281 was a more effective inhibitor than tropoelastin itself at the same molar concentration. In contrast, the scrambled peptide, which possessed an identical amino acid composition as peptide 246–281 but with a different organization, displayed no inhibitory effect.

Cell spreading on peptide 246–281 was highly variable (78.4 ± 37%) compared with tropoelastin (99.7 ± 0.6%) (Fig. 5Ci). This variability points to different functional orientations or conformations of the surface-bound peptide. On average, the area of spread cells on the peptide was significantly reduced by 76% than that on tropoelastin (Fig. 5Cii,iii). Moreover, unlike the full-length protein, peptide 246–281 did not promote increased cell proliferation over the no-protein/peptide control (Fig. 5D). The strong cell-adhesive property of peptide 246–281, contrasted with its moderate cell spreading and absent proliferative capabilities, suggests that this sequence may recapitulate initial contacts between cells and tropoelastin. Considering the lysine content of peptide 246–281, we propose that this sequence may also contact GAGs such as HS.

Peptide 246–281 adopts a mixture of conformations affected by temperature and solvent

Circular dichroism (CD) spectra of peptide 246–281 in phosphate buffer (PB) between 0 and 60 °C are shown in Fig. 6A. At 0 °C, the spectrum is characterized by a strong positive band at 190 nm and two negative bands at 202 and 222 nm. The spectrum is typical of a type I-III β-turn. Increasing the temperature to 25, 37, and 60 °C dramatically changes the spectral features. We observed the disappearance of the positive band and a slight blue-shift of the band at 202–200 nm. We conclude that at high temperatures poly-L-proline II helices mixed with more folded structures are present (e.g., turn). In Fig. 6B, the CD spectra of peptide 246–281 in 2,2,2-trifluoroethanol (TFE) are shown at the indicated temperatures. At 0 °C, the CD spectrum is characterized by a strong positive band at 190 nm and a small negative band at 206 nm together with a weak shoulder at 220 nm. Upon temperature increase, the CD spectra remain substantially unchanged except for a decrease in band intensity. Overall, the CD spectra in TFE are indicative of a stable α-helical/turn conformation, as expected in a solvent known to favor folded conformations.

Peptide 246–281 (1 mM) was also analyzed by 1D and 2D ^{1}H-NMR spectroscopy. Some insights on the secondary structure were obtained from the TOCSY and NOESY spectra, even if complete chemical shift assignment was hindered by the long overlapping alanine stretches and the high number of glycine residues. The fingerprint region of 2D TOCSY recorded at mixing time τ_m = 80 ms showed cross-peak patterns compatible with the amino acid residues present in the peptide sequence (Fig. 6C). The NH-amide signals of the alanine residues were in the range δ 8.30–7.95 p.p.m. The related H_α chemical shifts spanned a narrow region (δ 4.35–4.15 p.p.m.). The chemical shifts values for some of the H_α alanines were lower than those expected for typical random coil values (4.35 ± 0.1 p.p.m.), suggesting that some residues populate α-helical structures. The NH-amide signals of glycine residues are localized in the region from δ 8.57 to 8.23 p.p.m., while the H_α proton chemical shifts of all glycine residues are typical of random coil conformations. Only one glycine residue showed a large difference in the $H_{\alpha'}$ and $H_{\alpha''}$ chemical shifts, which suggests involvement in turn or turn-like structures.

HS triggers the adoption of β-strand conformation by Peptide 246–281

The interaction between peptide 246–281 and HS was investigated at 37 °C by carrying out CD measurements of the peptide as a function of HS concentration (Fig. 7A). In the absence of HS, the CD spectrum of peptide 246–281 shows a strong negative band centered at 200 nm and a weak shoulder at 221 nm, indicative of the presence of unordered conformations. Increasing HS concentration to 1, 10, and 50 μg·mL^{-1} decreased both the negative bands and the shoulder. At higher HS concentrations of 75 and 100 μg·mL^{-1}, a positive band at 190 nm appeared, suggesting the presence of regular conformations. Moreover, at 100 μg·mL^{-1} HS, a shoulder at 211 nm and a negative band at 216 nm were visible, indicating β-strand conformation. In summary, HS induces the net conformational transition of peptide 246–281 from an unordered to β-strand conformation, probably due to the neutralization of lysine side chains, which are positively charged at pH 7, by the negatively charged sulfated groups of HS. This β-strand conformation could also trigger aggregation through β-sheet interactions at high concentrations present in the solid state.

In order to check whether the interaction between peptide 246–281 and HS is specific, CD spectra of the scrambled peptide were carried out in the presence of increasing amounts of HS (Fig. 7B). The curves appear very similar, suggesting the permanence of unordered conformation. In order to establish if other sulfated sugars have the same ordering effect as HS,
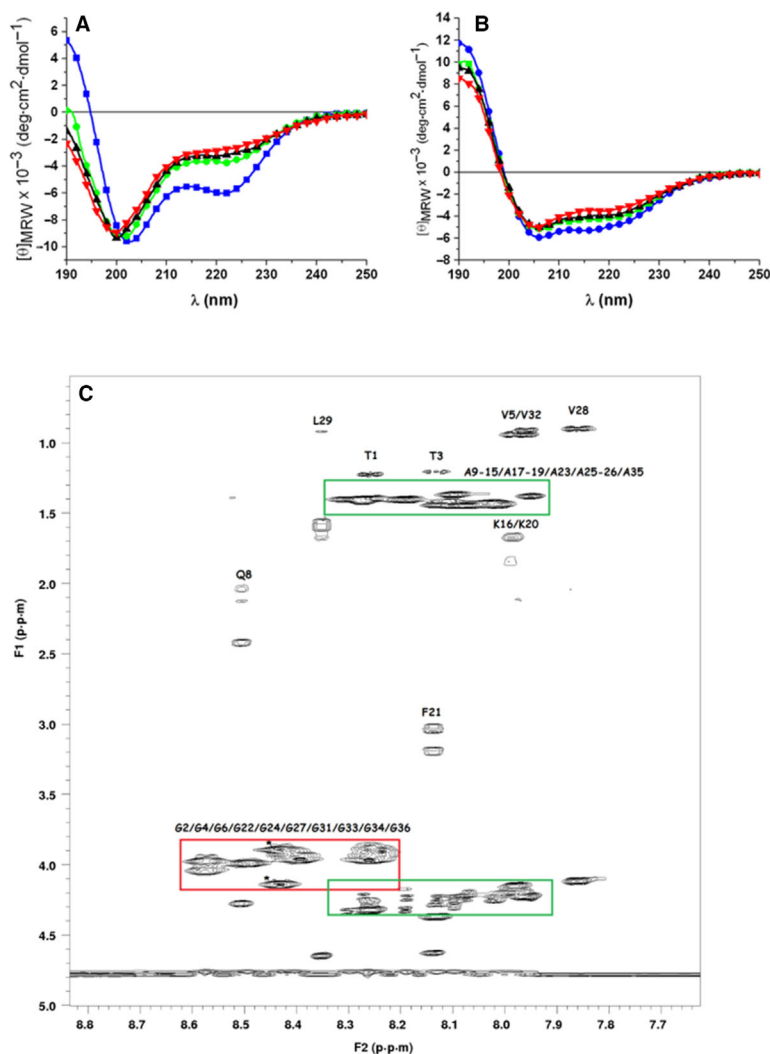
Fig. 6. CD spectra of peptide 246–281 in (A) PB or (B) TFE at the following temperatures: 0 °C (blue); 25 °C (green), 37 °C (black), and 60 °C (red). (C) Aliphatic-amide region of the TOCSY spectrum (τ_m = 80 ms) of peptide 246–281 recorded in 20 mM PBS, 0.2% NaN_3, and 0.1 mM 3-(trimethyl-sily1)-1-propane sulfonic acid in H_2O/D_2O, (90/10, v/v) at pH 6.0. Green boxes highlight the cross-peaks belonging to alanine residues, while the NH-H_α cross-peaks belonging to glycine residues are shown in red. Asterisks (*) indicate cross-peaks belonging to $H_{\alpha'}/H_{\alpha''}$ protons of a glycine that may participate in a turn structure.

CD data of peptide 246–281 at increasing amounts of CS were carried out (Fig. 7C). The data indicate the presence of unordered conformations for peptide 246–281 alone and in the presence of CS.

Given that the interaction between the peptide and HS was supposed to be electrostatic, we carried out CD measurements in the presence of 50 mM NaCl (Fig. 7A). The CD curve registered in the presence of salt was almost similar to the spectra carried out at lower HS concentrations (50 µg·mL^{-1}). Our interpretation is that ions from salt interrupt the peptide–glycosaminoglycan electrostatic interactions. Analogously, the spectra of Peptide 251–266, encoded by exon 15 of human tropoelastin and herein named EX15, were obtained in the presence of HS (Fig. 8A). The CD spectrum of EX15 was characterized by two negative bands: The stronger one centered at ~ 200 nm indicative of random coil conformation, and the weaker one

centered at ~ 222 nm, suggesting the presence of turn structures although in minor amounts. The addition of HS triggers the adoption of more folded conformations, as demonstrated by the decrease in the strong negative band at 200 nm. In fact, the reduction in intensity of the negative band was proportional to the increase in HS concentration. At the maximum concentration of HS, we observed a strong positive band at ~ 195 nm and a weak negative band at 220 nm. These spectra are diagnostic of type II β-turn. In summary, we conclude that the presence of HS induces a conformational transition of the peptide from unordered to folded conformations. Furthermore, in order to mimic the neutralization effect of HS on the lysine residues present in peptide 246–281, EX15 was studied by CD in aqueous solution as a function of pH. Accordingly, we observed a transition from unordered conformations at pH 7, due to repulsive interactions
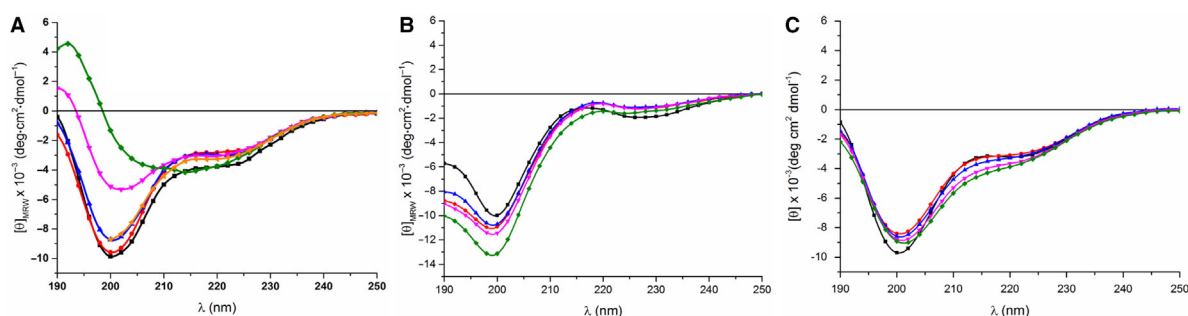
Fig. 7. CD spectra of (A) peptide 246–281 and (B) scrambled peptide 246–281 in PB at 37 °C, either alone (black squares), and in the presence of HS at the following concentrations: 10 µg·mL^{-1} (red circles); 50 µg·mL^{-1} (blue triangles), 75 µg·mL^{-1} (purple triangles), 100 µg·mL^{-1} (green diamonds), and 100 µg·mL^{-1} in 50 mM NaCl (orange triangles). (C) CD spectra of peptide 246–281 in PB at 37 °C, either alone (black squares), or in the presence of CS at the following concentrations: 10 µg·mL^{-1} (red circles), 50 µg·mL^{-1} (blue triangles), 75 µg·mL^{-1} (purple triangles), 100 µg·mL^{-1} (green diamonds).

among positively charged lysines, to more folded structures at pH 10, where lysine residues are uncharged (Fig. 8B).

HS enhances peptide 246–281 aggregation

NMR studies were performed to determine whether HS induced a conformational change in peptide 246–281. Comparison of the 1D-^{1}H spectra of peptide 246–281, recorded at the beginning and at the end of the 2D NMR spectra acquisitions, showed most (~ 85%) of the peptide was stable (Fig. 9A). When HS was added to a fresh sample of peptide 246–281, interactions were observed within 1 h. 2D TOCSY and NOESY experiments were performed on peptide 246–281 in the presence of HS. However, the low concentration of the residual soluble fraction of the peptide reduced the signal-to-noise ratio dramatically, thus preventing 2D spectra analysis and correlated conformational studies. At the end of the 2D spectra acquisition, signals due to peptide 246–281 showed a dramatic decrease, while the acetamido signals of HS had only slightly dropped (Fig. 9B). In order to monitor aggregation more easily by NMR, we reduced the

peptide and HS concentration to 0.3 and 0.1 mM, respectively.

In time-dependent studies of peptide 246–281 with HS, 1D ^{1}H-NMR spectra displayed significant changes. From top to bottom in Fig. 8A, the first spectrum refers to the initial stage of the aggregation process, whereas the last spectrum was recorded after 144 h when the aggregation was macroscopically visible. For all peaks of the peptide, we observed a systematic decrease in the signal intensity over time, while peaks belonging to the HS remain unaffected (Fig. 10A,C). No line broadening was evident for the observable signals throughout aggregation, suggesting that the decay of the signal represented a loss of peptide 246–281 rather than an increase in size of small oligomeric units. Furthermore, the spectra did not reveal additional signals that could come from low-molecular-weight intermediate states. Accordingly, the peptide monomers giving rise to detectable signals in liquid-state NMR experiments convert over time into larger, slowly tumbling aggregates with highly broadened and undetectable signals. When the peptide was analyzed in the absence of HS (Fig. 10B), the integration values of the peaks belonging to the peptide
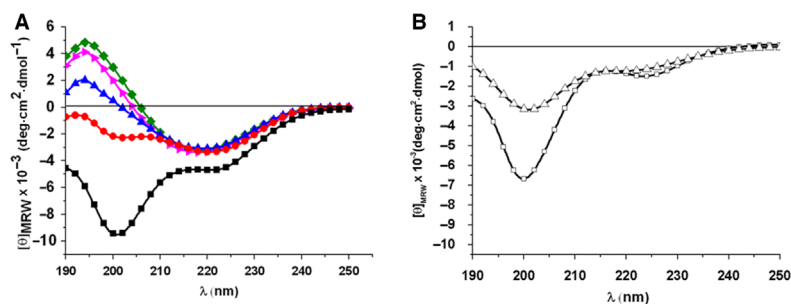
Fig. 8. (A) CD spectra at 37 °C in PB of EX15 (black) in the presence of HS at the following concentrations: 10 µg (red); 50 µg (blue), 75 µg (purple), 100 µg (green). (B) CD spectra of EX15 in aqueous solution at pH 7 (squares) and pH 10 (triangles).
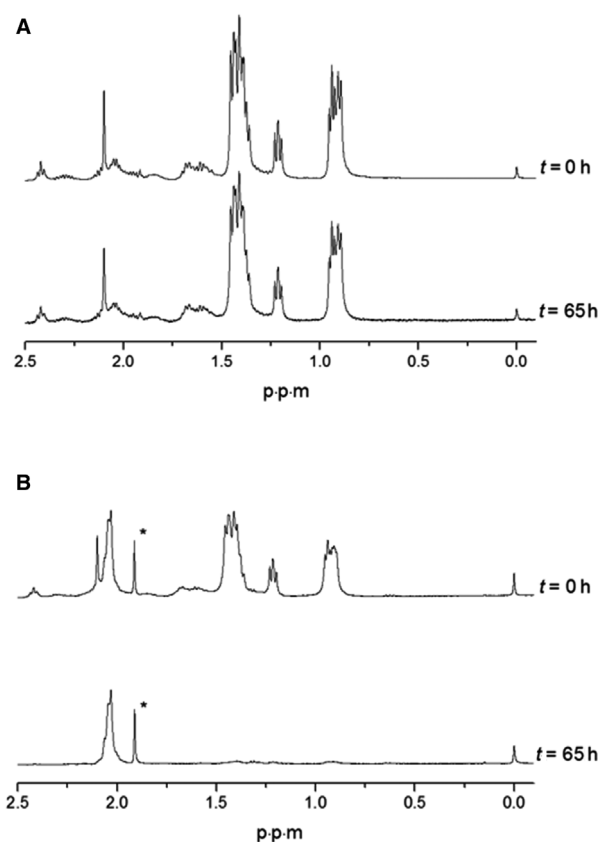
Fig. 9. Methyl region of the 1D 1H spectra of 1 mM peptide 246–281, either (a) alone or (b) with 0.3 mM HS at $t = 0$ h (top) and at $t = 65$h (bottom) after 2D acquisitions. Asterisks (*) indicate an impurity

(Fig. 10C) did not decrease, suggesting that aggregation either did not occur or proceeded very slowly. The CD and NMR data support a model where

association of peptide 246–281 was prompted by electrostatic interactions between the HS acidic groups with the protonated ε-amino groups of lysine residues in the peptide, and so facilitated the adoption of a β-strand conformation of peptide 246–281. In the absence of HS, peptide 246–281 populated different conformations (proposed as α-helix and unordered) that hindered this interaction.

Discussion

Cellular interactions with ECM proteins are crucial for cell survival and tissue maintenance. In contrast to other ECM proteins such as fibronectin and laminin, cellular interactions with tropoelastin are less understood. Tropoelastin has previously been reported to facilitate cell attachment and spreading via its C-terminal region and central domains 17–18 [3–7]. In particular, a sequence derived from domains 17–18 has been shown to directly support cell attachment through GAGs and cell spreading through integrins in a stepwise mechanism [7]. While the use of HS as a competitive inhibitor negated cell binding to this peptide, HS did not inhibit binding to N18, suggesting the presence of other cell-binding motifs upstream of domains 17–18.

Consistent with this hypothesis, the N16 tropoelastin construct still retains significant cell-adhesive and cell-spreading properties, although expectedly to a lower extent than N18 due to the missing domain 17–18 region. In contrast, this cell-interactive ability is lost in the N12 construct, therefore delineating the location of cell-contacting motifs to within domains 13–16. Accordingly, the 12–16 construct is at least functionally comparable to N16, confirming that the cell-interfacing site/s in the latter are primarily ensconced within the 12–16 region.
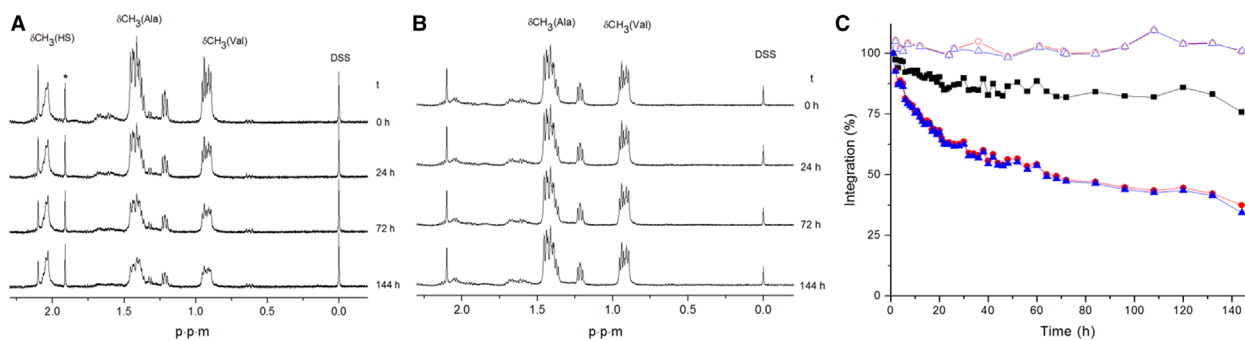
Fig. 10. Time-dependent NMR studies of peptide aggregation by 1D ^{1}H-NMR spectra. (A) Methyl region of 1D spectra of peptide 246–281 (0.3 mM) + HS (1 mM) recorded at different time points. (B) Methyl region of 1D spectra of peptide 246–281 (0.3 mM) recorded at different time points. (C) Aggregation kinetics monitored by integration of peptide and HS signals: -●- CH₃–Ala, -▲- CH₃–Val, -■- CH₃–HS of peptide 246–281 with HS, -○- CH₃–Ala, -△- CH₃–Val of peptide 246–281.

Cell interactions with the 12–16 construct are dominantly mediated by integrin receptors, as evidenced firstly by EDTA inhibition of cell adhesion, and validated by specific integrin-blocking antibodies. Cell adhesion to the 12–16 construct can be independently facilitated by either αV or α5β1 integrins, although αV integrins likely mediate initial contact, with α5β1 integrins participating subsequently. This sequential involvement of both integrin types is manifested by the more profound inhibitory effect of αV blocking over α5β1 blocking in cellular processes that occur over a longer time scale, that is, spreading. Blocking both αV and α5β1 completely inhibits cell spreading, indicating the coordinating roles of both types of integrins in this process. Although the 12–16 construct does not contain the canonical integrin-binding RGD motif, integrins are known to bind to a range of nonconsensus sequences, such as the collagen-derived GROGER and GFOGER motifs [9,10], or the vitronectin-derived KKQRFRHRNRKG sequence [11]. The two previously reported integrin-binding regions in tropoelastin, domains 17–18 and domain 36, also do not contain RGD, and instead feature alanines and lysines [7], or an RKRK motif [4], respectively.

The progressively increasing cell-adhesive capabilities of a series of tropoelastin constructs truncated after domains 12 to 16 (N12, N13, N14, N15.5, and N16) suggest the coordinated participation of each domain within this region. Nevertheless, cell attachment to N16 was halved in N14 and fully preserved in N15.5, while cell spreading to N16 was decreased by up to 78% in N14 and retained in N15.5, enabling the mapping of a major cell-interactive site to within domain 15 and the first half of domain 16. Due to the loss of contributions from domains 13 and 14, this region would not be expected to independently contain the full integrin-interfacing functionality previously characterized within the 12–16 construct.

Instead, we propose that this domain 15–16 region may capture some of the initial contacts between tropoelastin and cells. In line with this model, peptide 246–281, which encompasses this region, supported short-scale cell interactions such as cell adhesion and early-stage cell spreading, but not longer-scale processes such as cell proliferation. Moreover, the cell interactivity of peptide 246–281 was shown to be targeted and sequence-specific. Its sequence, characterized by a stretch of alanine and lysine, possesses similarities with that of Peptide 302–322 (AAAAAAAAAAKAA-KYGAAAGL), which is derived from the cell-adhesive domains 17–18 in tropoelastin [7]. Peptide 302–322 was previously found to interact with both GAGs and integrins αvβ3 and αvβ5 in a stepwise mechanism, with

lysine residues mediating contacts with GAGs. The lack of cell binding to the scrambled peptide 246–281, in which the native alanine/lysine stretch has been disrupted, suggests the functional significance of this motif. Furthermore, integrin blocking did not abolish cell adhesion to the 12–16 construct completely, suggesting the involvement of additional receptors such as GAGs during cell contact with this region of tropoelastin. That this relatively compact, 106-residue long domain 12–16 region is enriched for interactions with multiple cell receptors reflects other ECM peptides of comparable size with similar interactions. The 192-residue laminin α1 chain LG4 module and a 142-residue ADAM12 domain have also been shown to bind both GAGs (syndecans) and integrins [12,13].

The solvent-exposed, protruding position of peptide 246–281, near the tip of tropoelastin as depicted within the full-atomistic model [14], is consistent with its accessibility for intermolecular interactions with cell-surface receptors such as GAGs (Fig. 11). We propose that initial contacts between GAGs and the N-terminal segment of tropoelastin, which encompasses peptide 246–281, stabilize local tropoelastin conformation sufficiently to allow subsequent coordinated interactions between cells and the elastic matrix. Therefore, we investigated the conformation of peptide 246–281 and
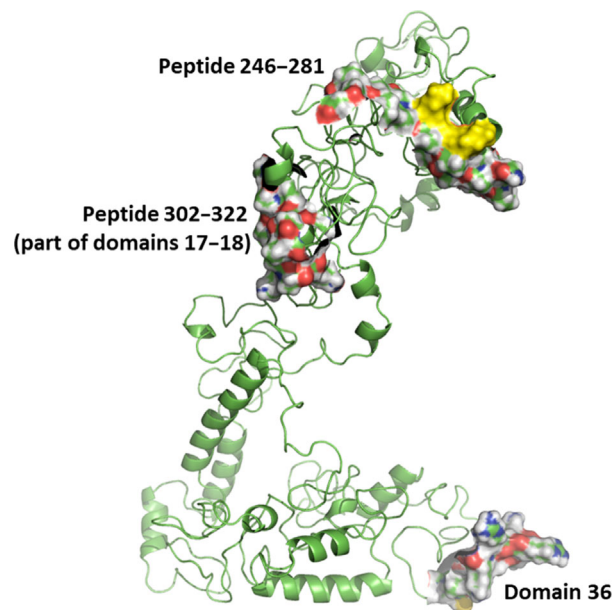
Fig. 11. Full-atomistic ribbon model of the tropoelastin molecule (green) [14] showing GAG- and/or integrin-binding sites: peptide 246–281 with lysine residues indicated in yellow, Peptide 302–322 within domains 17–18, and domain 36. The image was generated using PYMOL (Schrödinger, Inc., New York, NY, USA).

the effects of HS on peptide structure. The microenvironment that determines peptide conformation is not known *a priori* and can be different from the bulk macroscopic solution conditions (i.e., physiological conditions). Predicting the functional solvent environment for insoluble elastin is particularly difficult because the protein's hydrophobicity and highly cross-linked nature suggest a less polar internal environment than the surrounding solvent. For this reason, the experiments in this study were performed in both water and TFE. TFE is significantly less polar than water and is usually considered a structure-inducing solvent because it favors intramolecular hydrogen bonding, thus promoting folded conformations such as helices and turns [15–17]. While the actual local solution condition for insoluble elastin is unknown, it is likely to be intermediate between the two solvent extremes of water and TFE. At the molecular scale, CD demonstrated an ensemble of conformations comprising random coil, poly-L-proline II, and turn in aqueous solution, while α-helices dominated in the less polar TFE.

The presence of HS affects the secondary structure of peptide 246–281 by triggering a conformational transition toward β-strand conformation. This finding is consistent with a GAG-induced stabilization of tropoelastin local conformation to facilitate further cell-receptor contacts with other regions of tropoelastin, and potentially with other ECM components. Electrostatic interactions are expected to occur between the positively charged lysines of the peptide and the negatively charged HS chains. The neutralization of charges increases the hydrophobicity of the macromolecules and renders them prone to aggregation with HS. NMR results revealed that HS favors co-aggregates with the peptide, which was observed as precipitate at the end of the measurement. The effect of NaCl addition testifies to the electrostatic nature of the HS-peptide interaction. The addition of ionic salt interrupts this interaction and destroys the β-strand conformation. Previous studies have examined the involvement of lysine side chains in GAG interactions by treating tropoelastin with sulfosuccinimidyl acetate, which predominantly acetylates the epsilon amino group and neutralizes the charge [18]. Additional evidence that HS-induced conformational ordering of the peptide occurs via neutralization of lysine charges comes from CD analysis of peptide 246–281 as a function of pH (Fig. 8). At physiological pH, in which lysines are positively charged, peptide 246–281 populated unordered conformations. At high pH, in which lysines are uncharged and thus mimic charge neutralization by HS, peptide 246–281 displayed more folded

conformations. On this basis, we infer that HS stabilizes tropoelastin local conformation at contact sites, via charge interactions with tropoelastin lysine residues.

The presence of nonpolar residues in peptide 246–281 does not affect the coupling between HS and the few lysines present in the peptide sequence. CD spectra carried out on EX15, which contains the lysine motif in peptide 246–281, showed analogous spectral features in the presence of HS. This finding led us to speculate that most of the negative charges of HS are neutralized by the two lysines of the peptide 246–281, probably in a 1 : 1 ratio. This interaction with HS is specific, as the conformation of the scrambled peptide does not change in the presence of GAG molecules. Furthermore, the conformation of peptide 246–281 remains unchanged with increasing amounts of CS, another type of GAG. A recent study has demonstrated that domain 15 is only partly and heterogeneously involved in tropoelastin cross-linking, which suggests the availability of at least one of the lysines for binding to HS chains [19].

The incorporation of lysine into integrin-adhesive peptides such as RGD improves their cell adhesion performance [20]. Accordingly, the lysine-rich sequences of tropoelastin could be used to improve the biocompatibility of cell-interfacing materials. This study represents the first experimental evidence of direct interactions between tropoelastin lysine residues and HS, which comprises ∼ 30% of the soluble component of purified elastin. These results add to our comprehension of the complex mechanisms of interaction between tropoelastin, cells, and ECM components. Although it is difficult to say whether an increase in HS in elastic fibers is correlated with age, HS appeared particularly concentrated in the mineralization front of dermal elastic fibers in patients affected by pseudoxanthoma elasticum (PXE) [8]. Our results here showed that HS triggers a conformational transition of peptide 246–281 from unordered to β-strand conformation, pointing to structural stabilization that potentially predisposes to additional cell-ECM interactions. We propose that domains 14–16 direct initial cell attachment through cell-surface HS GAGs, followed by αV and α5β1 integrin-promoted attachment and spreading on domains 12–16 of tropoelastin. This type of two-step mechanism involving GAGs and integrins follows that recently shown for the central domains 17–18 of tropoelastin [7]. This replication of the mechanism, but with a different sequence, raises the attractive possibility that multiple sites in tropoelastin work in a coordinated manner to promote cell attachment cooperatively. Sequences in

domains 12–16, 17–18 [5,7], and 36 [3,4] interface with both GAGs and integrins (Fig. 11). The VGVAPG repeats predominantly in domain 24, or GxxPG motifs in elastin-derived peptides activate the elastin receptor complex. These receptor interactions trigger cell events such as chemotaxis, migration, adhesion, proliferation, protein secretion, and angiogenesis [21]. Discovering the functional roles of specific tropoelastin sequences would enhance our understanding of the signaling events underpinning elastin-induced wound healing, which has the potential to enhance the design of biomaterials and advance current technologies in tissue regeneration.

Materials and methods

Tropoelastin expression

Recombinant human tropoelastin constructs were produced in-house. Tropoelastin constructs N18 (aa 27–365), N16 (aa 27–296), N15.5 (aa 27–281), N14 (aa 27–236), N13 (aa 27–216), N12 (aa 27–202), N10 (aa-27–168), and 12–16 (aa 203–296) were modified from the WT full-length tropoelastin sequence corresponding to amino acid residues 27–724 of GenBank accession number AAC98394 (gi 182020). The gene sequences corresponding to these constructs were cloned in-house into the pET3d vector, transformed into *Escherichia coli* BL21 (DE3) cells, overexpressed, isolated as described [22], and purified by reversed-phase HPLC using an Agilent Technologies ZORBAX StableBond 300SB-C18 5 μm column. A gradient of 0–100% acetonitrile and 0.1% TFA over 1 h was used to elute the fractions. Single species corresponding to predicted molecular masses were isolated and confirmed using SDS/PAGE.

Peptide synthesis and purification

Peptide sequences of EX15, peptide 246–281, and scrambled peptide 246–281 are derived from the human tropoelastin sequence and were made by solid-phase peptide synthesis (SPPS). EX15 has the sequence GVGPQ AAAAAAAKAAAKF and was synthesized as previously described [23].

Peptide 246–281 has the sequence Ac-TGTGVGPQAAAAAAAKAAAKFGAGAAGVLPGVG-GAG-NH$_2$. The scrambled peptide 246–281 has the sequence Ac-AVQAPAKLATAAGAGGAFAGGAGGV-GAKGATAVPAG-NH$_2$. Both variants were acetylated at the N terminus and amidated at the C terminus, and were synthesized by SPPS on a tribute automatic peptide synthesizer (Gyros Protein Technologies Inc., Tucson, AZ, USA) with a standard 9-fluorenylmethoxycarbonyl (Fmoc) protection peptide synthesis protocol [24]. Cleavage of the peptides from the resin and for amino acid side-chain

protecting groups was achieved by using H$_2$O (95% TFA) together with phenol, and thioanisole. The peptides were lyophilized and purified by reverse phase HPLC. A binary gradient was used, and the solvents were H$_2$O (0.1% TFA) and CH$_3$CN (0.1% TFA).

Mass spectrometry

Purity of the peptides was assessed by High Resolution Mass Spectrometry (HRMS) utilizing Matrix-Assisted Laser Desorption Ionization Time of Flight (MALDI-TOF) mass spectrometry.

Ac-TGTGVGPQAAAAAAAKAAAKFGAGAAGVLP GVGGAG-NH$_2$. HRMS (MALDI): m/z 2962.52 g·mol^{-1} [M + H]$^+$, m/z 2984.50 g·mol^{-1} [M + Na]$^+$, m/z 3000.51 g·mol^{-1} [M + K]$^+$, 2962.59 g·mol^{-1} calculated for [C$_{129}$H$_{213}$N$_{40}$O$_{40}$]$^+$

Ac-AVQAPAKLATAAGAGGAFAGGAGGVGAKGAT AVPAG-NH$_2$. HRMS (MALDI): m/z 2962.91 g·mol^{-1} [M + H]$^+$, 2962.59 g·mol^{-1} calculated for [C$_{129}$H$_{213}$N$_{40}$O$_{40}$]$^+$

Substrate coating

Tissue culture wells were incubated with stated molar concentrations of either full-length tropoelastin or peptide 246–281 at 4 °C overnight. Wells were washed with PBS (10 mM sodium phosphate, 150 mM NaCl, pH 7.4) to remove unbound protein or peptide.

Cell culture

GM3348 human dermal fibroblasts (Coriell Research Institute, Camden, NJ, USA) were cultured in Dulbecco's modified Eagle's medium (DMEM) supplemented with 10% (v/v) fetal bovine serum and 1% (v/v) penicillin/streptomycin. These cells were used for all cell-based assays described subsequently.

Cell attachment

Wells coated with tropoelastin constructs or peptide 246–281 were blocked with 10 mg·mL^{-1} heat-denatured bovine serum albumin for 1 h to minimize contact between seeded cells and the underlying tissue culture plastic. Wells were seeded with 20 000 cells·cm^{-2} in serum-free DMEM. Where indicated, peptide 246–281 or a scrambled peptide was added into wells to inhibit cell attachment to the underlying tropoelastin substrate. Cells were incubated for 1 h at 37 °C in a 5% CO$_2$ incubator. Nonadhered cells were washed off with PBS. Adhered cells were fixed with 3% (v/v) formaldehyde for 20 min, washed with PBS, and then stained with 0.1% (w/v) crystal violet in 0.2 m 2-(N-morpholino)ethanesulfonic acid buffer for 1 h. Excess stain was removed with multiple washes of reverse osmosis

water. Cell staining was solubilized with 10% (v/v) acetic acid, and absorbance values were read at 570 nm in a plate reader.

Cell spreading

Wells were prepared as described for the cell attachment assay and seeded with 10^5 cells·mL^{-1}. After a 1–1.5 h of incubation, cells were fixed directly with 3% (v/v) formaldehyde and visualized by phase-contrast microscopy with a Zeiss Axiovert.A1 microscope (Carl Zeiss AG, Oberkochen, Germany) at 10× magnification, and images were taken on a microscope camera (AxioCam IC 1; Carl Zeiss AG) for quantification. The degree of cell spreading was measured using a yes/no threshold. Cells with a flattened phase-dark body with visible nucleus and filopodia/lamellipodia were considered spread, whereas cells that were rounded and phase-bright were considered unspread. Where indicated, the area of cells classified as 'spread' was measured using ImageJ to determine the degree of spreading.

Antibody inhibition

Antibody inhibition studies were conducted following cell attachment or spreading assay protocols as described above. As an inhibitor, α-lactose, HS, or EDTA was added to cells at a concentration of 10 mM, 10 μg·mL^{-1}, and 5 mM, respectively. The molecular weight of HS was 10–70 kDa, and the sulfate per hexosamine was 0.8–1.8. Antibodies against human αV and β8 integrins (Abcam, Cambridge, UK) were added to cells at 20 μg·mL^{-1}. The antibody against α5β1 integrin (JBS5; Millipore, Burlington, MA, USA) was added at either one in 50 or one in 100 dilution.

Cell proliferation

Wells were prepared as described for the cell attachment assay and seeded with 5000 cells·cm^{-2}. Cells were fixed at 1, 4 and 7 days postseeding, and quantified via crystal violet staining.

CD spectroscopy

Circular dichroism spectra of peptides were acquired at different temperatures with a Jasco J-815 (Easton, MD, USA) Spectropolarimeter equipped with a HAAKE thermostat as temperature controller. Samples were solubilized at a concentration of 0.1 mg·mL^{-1} in 10 mM sodium phosphate, pH 7.0 (PB) and in TFE. Milli-Q (Burlington, MA, USA) water was used to prepare all the solutions, and the solutions were pipetted in a 0.1 cm path length quartz cell. Samples were equilibrated at the desired temperature for 2 min before acquisition. Spectra

were acquired by taking points every 0.1 nm, with 100 nm·min^{-1} scan rate, 16 scans, an integration time of 2 s, and a 1 nm bandwidth. The data are expressed in terms of $[\theta]_{MRW}$, the mean residue ellipticity value, as deg cm^2·dmol^{-1}, in order to compare the data obtained for different peptide lengths. When CD spectroscopy was performed in the presence of HS (MW 10 300; SO$_3$/COO$^-$ ratio 1.4) and CS (MW 2330; SO$_3$/COO$^-$ ratio 0.93), both kindly donated by Opocrin SpA Research Laboratories, Corlo, Modena, Italy, measurements were performed at 37 °C as previously described. The effect of HS on CD was assessed following the addition of 10–100 μg·mL^{-1} HS.

NMR spectroscopy

NMR investigation was performed on peptide 246–281 dissolved in 20 mM PBS, 0.2% NaN$_3$, and 0.1 mM 3-(trimethyl-silyl)-1-propane sulfonic acid in H$_2$O/D$_2$O, (90/10, v/v) at pH 6.0. All NMR experiments were performed on a Varian Unity INOVA 500 MHz spectrometer equipped with a 5 mm triple-resonance probe and z-axial gradients. In all experiments, the temperature was controlled to 298 K. For conformational studies, one- and two-dimensional spectra were acquired on fresh peptide 246–281 at 1 mM concentration in the presence and absence of 0.3 mM HS. One-dimensional spectra were acquired in Fourier mode with quadrature detection, and the water signal was suppressed by double-pulsed field-gradient spin-echo. Two-dimensional and NOESY spectra were collected in the phase-sensitive mode using the States method. Typical data were 2048 complex data points, 64 transients and 256 increments. Relaxation delays were set to 2.5 s, and spinlock (MLEV-17) mixing time was 80 ms for TOCSY and 200–300 ms for NOESY experiments. Shifted sine bell squared weighting and zero filling to 2K × 2K was applied before Fourier transform. Peptide aggregation was monitored by recording one-dimensional 1H spectra on peptide 246–281 (0.3 mM) in the presence and absence of HS (0.1 mM) each hour for 140 h. Data were processed with VNMRJ 2.2D. Integrals of selected regions were measured after exponential (LB = 0.5 Hz) window function application, FT transformation, and baseline correction. The integrals of the signals were compared to the 3-(trimethyl-silyl)-1-propane sulfonic acid signal with arbitrary integral value of 1.

Statistical analyses

Experiments were performed in triplicate or quadruplicate as indicated and reported as mean ± standard deviation of mean (SD). Analyses were carried out using one-way or two-way analysis of variance (ANOVA) applied with Bonferroni post-tests. Data were accepted as statistically

significant at $P < 0.05$ (*$P < 0.05$, **$P < 0.01$, ***$P < 0.001$, and ****$P < 0.0001$).

Acknowledgements

Conflict of interest

ASW is the Scientific Founder of Elastagen Pty Ltd, now sold to Allergan and AbbVie. All other authors declare no conflict of interest.

Author contributions

BB, GCY, PL, DE, AP, AL, and NC planned and performed experiments. BB, GCY, PL, DE, AP, DQ, and ASW analyzed data. BB, GCY, PL, and ASW wrote the paper.

Peer Review

The peer review history for this article is available at https://publons.com/publon/10.1111/febs.15702.

References

1 Wise SG, Yeo GC, Hiob MA, Rnjak-Kovacina J, Kaplan DL, Ng MKC & Weiss AS (2014) Tropoelastin: a versatile, bioactive assembly module. *Acta Biomater* **10**, 1532–1541.

2 Hinek A, Keeley FW & Callahan J (1995) Recycling of the 67-kDa elastin binding protein in arterial myocytes is imperative for secretion of tropoelastin. *Exp Cell Res* **220**, 312–324.

3 Broekelmann TJ, Kozel BA, Ishibashi H, Werneck CC, Keeley FW, Zhang L & Mecham RP (2005) Tropoelastin interacts with cell-surface glycosaminoglycans via Its COOH-terminal domain. *J Biol Chem* **280**, 40939–40947.

4 Bax DV, Rodgers UR, Bilek MMM & Weiss AS (2009) Cell adhesion to tropoelastin is mediated via the C-terminal GRKRK motif and integrin alphaVbeta3. *J Biol Chem* **284**, 28616–28623.

5 Lee P, Bax DV, Bilek MMM & Weiss AS (2014) A novel cell adhesion region in tropoelastin mediates attachment to integrin αVβ5. *J Biol Chem* **289**, 1467–1477.

6 Rodgers UR & Weiss AS (2004) Integrin alpha v beta 3 binds a unique non-RGD site near the C-terminus of human tropoelastin. *Biochimie* **86**, 173–178.

7 Lee P, Yeo GC & Weiss AS (2017) A cell adhesive peptide from tropoelastin promotes sequential cell attachment and spreading via distinct receptors. *FEBS J* **284**, 2216–2230.

8 Gheduzzi D, Guerra D, Bochicchio B, Pepe A, Tamburro AM, Quaglino D, Mithieux S, Weiss AS & Pasquali Ronchetti I (2005) Heparan sulphate interacts with tropoelastin, with some tropoelastin peptides and is present in human dermis elastic fibers. *Matrix Biol* **24**, 15–25.

9 Kim JK, Xu Y, Xu X, Keene DR, Gurusiddappa S, Liang X, Wary KK & Höök M (2005) A novel binding site in collagen type III for integrins alpha1beta1 and alpha2beta1. *J Biol Chem* **280**, 32512–32520.

10 Zhang WM, Kapyla J, Puranen JS, Knight CG, Tiger CF, Pentikainen OT, Johnson MS, Farndale RW, Heino J & Gullberg D (2003) alpha 11beta 1 integrin recognizes the GFOGER sequence in interstitial collagens. *J Biol Chem* **278**, 7270–7277.

11 Vogel BE, Lee SJ, Hildebrand A, Craig W, Pierschbacher MD, Wong-Staal F & Ruoslahti E (1993) A novel integrin specificity exemplified by binding of the alpha v beta 5 integrin to the basic domain of the HIV Tat protein and vitronectin. *J Cell Biol* **121**, 461–468.

12 Hozumi K, Suzuki N, Nielsen PK, Nomizu M & Yamada Y (2006) Laminin α1 chain LG4 module promotes cell attachment through syndecans and cell spreading through integrin α2β1. *J Biol Chem* **281**, 32929–32940.

13 Iba K, Albrechtsen R, Gilpin B, Fröhlich C, Loechel F, Zolkiewska A, Ishiguro K, Kojima T, Liu W, Langford JK *et al.* (2000) The cysteine-rich domain of human ADAM 12 supports cell adhesion through syndecans and triggers signaling events that lead to beta1 integrin-dependent cell spreading. *J Cell Biol* **149**, 1143–1156.

14 Tarakanova A, Yeo GC, Baldock C, Weiss AS & Buehler MJ (2018) Molecular model of human tropoelastin and implications of associated mutations. *Proc Natl Acad Sci USA* **115**, 7338–7343.

15 Bodkin MJ & Goodfellow JM (1996) Hydrophobic solvation in aqueous trifluoroethanol solution. *Biopolymers* **39**, 43–50.

16 Buck M (1998) Trifluoroethanol and colleagues: cosolvents come of age. Recent studies with peptides and proteins. *Q Rev Biophys* **31**, 297–355.

17 Reiersen H & Rees AR (2000) Trifluoroethanol may form a solvent matrix for assisted hydrophobic

interactions between peptide side chains. *Protein Eng Des Sel* **13**, 739–743.

18 Wu WJ, Vrhovski B & Weiss AS (1999) Glycosaminoglycans mediate the coacervation of human tropoelastin through dominant charge interactions involving lysine side chains. *J Biol Chem* **274**, 21719–21724.

19 Schräder CU, Heinz A, Majovsky P, Karaman Mayack B, Brinckmann J, Sippl W & Schmelzer CEH (2018) Elastin is heterogeneously cross-linked. *J Biol Chem* **293**, 15107–15119.

20 Luo K, Mei T, Li Z, Deng M, Zhang Z, Hou T, Dong S, Xie Z, Xu J & Luo F (2016) A high-adhesive lysine-cyclic RGD peptide designed for selective cell retention technology. *Tissue Eng Part C Methods* **22**, 585–595.

21 Scandolera A, Odoul L, Salesse S, Guillot A, Blaise S, Kawecki C, Maurice P, El Btaouri H, Romier-Crouzet B, Martiny L *et al.* (2016) The elastin receptor complex: a unique matricellular receptor with high anti-tumoral potential. *Front Pharmacol* **7**(32), 1–10. https://doi.org/10.3389/fphar.2016.00032

22 Martin SL, Vrhovski B & Weiss AS (1995) Total synthesis and expression in *Escherichia coli* of a gene encoding human tropoelastin. *Gene* **154**, 159–166.

23 Tamburro AM, Pepe A & Bochicchio B (2006) Localizing α-helices in human tropoelastin: assembly of the elastin "Puzzle". *Biochemistry* **45**, 9518–9530.

24 Bochicchio B, Pepe A, Crudele M, Belloy N, Baud S & Dauchez M (2015) Tuning self-assembly in elastin-derived peptides. *Soft Matter* **11**, 3385–3395.